Computer Assisted Methods in Engineering and Science, **23**: 87–107, 2016.

A comparison between the improved element-free Galerkin method and the element-free Galerkin method for 2D potential and elasticity problems

Imen Debbabi, Zohra Sendi, Hédi BelHadjSalah
LGM, ENIM, University of Monastir
Monastir, Tunisia
e-mail: imen.debbabi86@gmail.com, zohrasendii@yahoo.fr, hedi.belhadjsalah1@gmail.com

In this paper, a comparison between the improved element-free Galerkin (IEFG) method, based on the improved moving least square (IMLS) approximation, and the element-free Galerkin (EFG) method, based on the moving least square (MLS) approximation, is presented. The IMLS approximation is obtained when an orthogonal basis function with a weight function is used. The IMLS approximation has a greater computational efficiency than the existing MLS approximation and does not lead to an ill-conditioned system of equations. The comparison is made for two-dimensional (2D) potential problems and 2D elastic problems. From these problems, the efficiency of the IEFG method is validated by comparing the results obtained with the IEFG method and EFG method with those obtained analytically.

Keywords: EFG method, potential problems, elasticity problems, IMLS approximation.

1. Introduction

Accurate and efficient numerical simulation is usually sought to study engineering problems. These problems are always solved by traditional computational methods. Unfortunately, these methods cannot be effectively applied in some complex problems such as large deformation especially when damaged domains exist, dynamic fracturing or explosion problems. In fact for these problems the presence of distorted meshes does not enable obtaining correct solution. To deal with this problem, meshing and remeshing techniques are used, but these techniques are very time consuming. So, in some of these cases, because the problem is related to the mesh itself, meshless methods have shown good efficiency [1–5].

In recent years, meshless techniques have attracted the attention of researchers; the main objective of mesh free methods, when compared with the traditional finite element method, is to reduce the difficulty of meshing and remeshing the whole structure by simply adding nodes. The differences between meshless and conventional methods are in how the studied domain is discretized and how the shape functions are formulated. When these two steps are accomplished, the final discrete equations are obtained in the same way. There is a variety of mesh free methods, and the smoothed-particle hydrodynamics method is the first meshless method and it was proposed by Monaghan [6] and Lucy [7] in 1977. Since that time, many meshless methods had been developed such as the diffuse element method (DEM) proposed by Nayrols [8] and the element-free Galerkin (EFG) method proposed by Belytschko et al. [9]. Duarte and Oden developed the *h-p* clouds [10], and Atluri proposed the meshless local Petrov-Galerkin (MLPG) method [11]. The difference between all of these methods depends on the approximation techniques.

The EFG method, one of the most well-known and applied methods, is based on the MLS approximation. This method has shown efficiency and good accuracy but it is agreed that it is time consuming [12]. This large CPU time is mainly caused by the inversion of the so-called moment

matrix, when the problem is solved. In addition, the use of the EFG method leads sometimes to an ill-conditioned system of equations and an accurate solution becomes difficult to obtain [13]. To avoid these difficulties, the IEFG method, based on the IMLS approximation, is presented in [14]. In the IMLS, the orthogonal function system with a weight function is used as the basis function [15]. These weighted basis functions lead to a diagonal moment matrix which it inverse is directly calculated. This advantage gives a greater computational speed and efficiency [16].

In this paper, a comparison between the IEFG method and EFG method is presented. To achieve this comparison, the MLS and IMLS approximations are first presented, and then the IEFG method is discussed for potential and elastic problems. Finally, numerical 2D potential and elastic problems are presented to demonstrate the efficiency of the IEFG method in comparison with the EFG method.

2. MLS approximation

2.1. MLS interpolants functions

In the EFG method, the MLS approximation is used to construct the shape functions. For a field variable $u(x)$ defined in the domain Ω, the approximation of $u(x)$ denoted $u^h(x)$ is

$$u^h(x) = \sum_{i=1}^{m} p_i(x)a_i(x) = p^T(x)a(x), \tag{1}$$

where $p(x)$ is a vector of monomial basis functions, m is the number of terms in the basis and $a(x)$ is a vector of coefficients of the basis functions. In general, the basis functions are as follows:

- Linear basis

  $p^T(x) = (1, x_1)$ in 1D,

  $p^T(x) = (1, x_1, x_2)$ in 2D.

- Quadratic basis

  $p^T(x) = (1, x_1, x_1^2)$ in 1D,

  $p^T(x) = (1, x_1, x_2, x_1^2, x_1x_2, x_2^2)$ in 2D.

  The vector of coefficient $a(x)$ is defined by

  $a^T(x) = (a_1(x), a_2(x), \ldots, a_m(x))$.

  The local approximation of the function $u(x)$ as given by Lancaster and Salkauskas [17] is

$$u^h(x, \overline{x}) = \sum_{i=1}^{m} p_i(\overline{x})a_i(x) = p^T(\overline{x})a(x). \tag{2}$$

In the case of the MLS approximation $\overline{x}$ can be chosen arbitrary and thus it can be the node position x_I. To obtain the local approximation of $u(x)$, the difference between the local approximation $u^h(x, x_I)$ and $u(x_I)$ must be minimized by a weighted least square method.

Define a function

$$J(a, x) = \sum_{I}^{n} w(x - x_I)\left[u^h(x, x_I) - u(x_I)\right]^2 = \sum_{I}^{n} w(x - x_I)\left[\sum_{i=1}^{m} p_i(x_I)a_i(x) - u(x_I)\right]^2, \tag{3}$$

where $w(x-x_I)$ is the weight function with a domain of influence, and x_I, $I=1,2,\ldots,n$ are the nodes in the domain of influence that covers x.

Equation (3) can be written as

$$J(a,x)=(pa(x)-u)^T W(x)\,(pa(x)-u)\,, \tag{4}$$

where

$$u^T=(u_1,u_2,\ldots,u_n) \quad \text{and} \quad u_i=u(x_i), \tag{5}$$

$$p=\begin{bmatrix} p_1(x_1) & p_2(x_1) & \cdots & p_m(x_1) \\ p_1(x_2) & p_2(x_2) & & p_m(x_2) \\ \vdots & & \ddots & \vdots \\ p_1(x_n) & p_2(x_n) & \cdots & p_m(x_n) \end{bmatrix}, \tag{6}$$

$$W(x)=\begin{bmatrix} w\,(x-x_1) & 0 & \cdots & 0 \\ 0 & w\,(x-x_2) & & 0 \\ \vdots & & \ddots & \vdots \\ 0 & 0 & \cdots & w\,(x-x_n) \end{bmatrix}. \tag{7}$$

The minimization condition requires

$$\frac{\partial J(a,x)}{\partial a}=0, \tag{8}$$

which gives the equation system

$$A(x)a(x)=B(x)u. \tag{9}$$

Knowing that matrices $A(x)$ and $B(x)$ are given by the following rules:

$$A(x)=p^T W(x)p, \tag{10}$$

$$B(x)=p^T W(x) \tag{11}$$

and u is the vector of nodal values, using Eq. (9) we can write

$$a(x)=A^{-1}B(x)u. \tag{12}$$

The expression of $u^h(x)$ is given by

$$u^h(x)=\Phi(x)u=\sum_I^n \Phi_I(x)u_I, \tag{13}$$

where $\Phi(x)$ is the vector of the MLS shape functions defined by

$$\Phi(x)=p^T(x)A^{-1}(x)B(x). \tag{14}$$

2.2. The orthogonal basis functions

In the IMLS approximation, to avoid the problem that the equation system (9) is sometimes ill-conditioned, the basis functions are chosen to be weighted orthogonal.

In the Hilbert space span (p), for the set of point $\{x_i\}$ and the weight functions w_i, if the functions $p_1(x),p_2(x),\ldots,p_m(x)$ satisfy the condition (15) below, then the function set is called a weighted orthogonal function set with a weight function $\{w_i\}$ about point $\{x_i\}$ In the case where

$p_1(x), p_2(x), \ldots, p_m(x)$ are polynomials the function set $p_1(x), p_2(x), \ldots, p_m(x)$ is called a weighted orthogonal polynomial set with the weight function $\{w_i\}$ about point $\{x_i\}$.

$$(p_k, p_j) = \sum_{i=1}^{n} w_i p_k(x_i) p_j(x_i) = \begin{cases} 0, k \neq j \\ A_k, k = j \end{cases} \quad (k, j = 1, 2, \ldots, m) \,. \tag{15}$$

Using Eq. (15), Eq. (9) can be written as

$$\begin{bmatrix} (p_1,p_1) & (p_1,p_2) & \cdots & (p_1,p_m) \\ (p_2,p_1) & (p_2,p_2) & & (p_2,p_m) \\ \vdots & & \ddots & \vdots \\ (p_m,\ p_1) & (p_m,p_2) & \cdots & (p_m,p_m) \end{bmatrix} \begin{bmatrix} a_1(x) \\ a_2(x) \\ \vdots \\ a_m(x) \end{bmatrix} = \begin{bmatrix} (p_1,u) \\ (p_2,u) \\ \vdots \\ (p_m,u) \end{bmatrix}. \tag{16}$$

If the basis function set is a weighted orthogonal function set, then Eq. (16) has this expression

$$\begin{bmatrix} (p_1,p_1) & 0 & \cdots & 0 \\ 0 & (p_2,p_2) & & 0 \\ \vdots & & \ddots & \vdots \\ 0 & 0 & \cdots & (p_m,p_m) \end{bmatrix} \begin{bmatrix} a_1(x) \\ a_2(x) \\ \vdots \\ a_m(x) \end{bmatrix} = \begin{bmatrix} (p_1,u) \\ (p_2,u) \\ \vdots \\ (p_m,u) \end{bmatrix}, \tag{17}$$

$a_i(x)$ are then directly obtained from (17):

$$a_i(x) = \frac{(p_i, u)}{(p_i, p_i)}, \qquad (i = 1, 2, \ldots, m). \tag{18}$$

Then

$$a(x) = \overline{A}(x) B(x) u, \tag{19}$$

where

$$\overline{A}(x) = \begin{bmatrix} \dfrac{1}{(p_1,p_1)} & 0 & \cdots & 0 \\ 0 & \dfrac{1}{(p_2,p_2)} & & 0 \\ \vdots & & \ddots & \vdots \\ 0 & 0 & \cdots & \dfrac{1}{(p_m,p_m)} \end{bmatrix}. \tag{20}$$

$\overline{A}(x)$, denoted A^{-1} in the MLS approximation, is a diagonal matrix that cannot lead to an ill-conditioned system equations. Coefficients $a(x)$ are also directly and simply obtained. The approximation $u^h(x)$ has then the following expression:

$$u^h(x) = \overline{\phi}(x) u = \sum_{I=1}^{n} \overline{\phi}_I(x) u_I, \tag{21}$$

$$\overline{\Phi}(x) = p^T(x) \overline{A}(x) B(x). \tag{22}$$

The Schmidt method can be used to form a weighted orthogonal basis from an arbitrary basis function $\overline{p}$, if the monomial basis function p, for example, is

$$p = (p_i) = \left(1, x_1, x_2, x_1^2, x_1 x_2, x_2^2\right). \tag{23}$$

The weighted orthogonal basis function can be defined by

$$\overline{p}_i = p_i - \sum_{k=1}^{i-1} \frac{(p_i, \overline{p}_k)}{(\overline{p}_k, \overline{p}_k)} \overline{p}_k, \qquad i = 1, 2, 3, \ldots. \tag{24}$$

The first derivative of $\overline{p}_i$ denoted $\overline{p}_{i_{,x}}$ is given by

$$\overline{p}_{i_{,x}} = p_{i_{,x}} - \sum_{k=1}^{i-1} \left[\frac{(p_i, \overline{p}_k)_{,x} (\overline{p}_k, \overline{p}_k) - (p_i, \overline{p}_k) (\overline{p}_k, \overline{p}_k)_{,x}}{(\overline{p}_k, \overline{p}_k)^2} \overline{p}_k + \frac{(p_i, \overline{p}_k)}{(\overline{p}_k, \overline{p}_k)} \overline{p}_{k_{,x}} \right]. \tag{25}$$

2.3. Weight function

The weight function is non-zero only over a small neighborhood of a node x_I. This neighborhood is called the domain of influence of node I. The common weight functions used in the literature are cubic spline function, fourth-order spline function and the exponential weight function. In this paper, we choose to use the fourth-order spline function given by

$$w(s) = \begin{cases} 1 - 6s^2 + 8s^3 - 3s^4, & |s| \le 1, \\ 0 & |s| \ge 1, \end{cases} \tag{26}$$

where $s = \dfrac{\|x - x_I\|}{d}$ and $\|x - x_I\|$ is the distance from a sampling point x to a node x_I, and d is the size of the domain of influence of the I-th node.

In the case of a circular domain $d = a_c d_i$, where d_i is the average distance between nodes and a_c is a scaling parameter chosen large enough so that the stiffness matrix can be regular.

3. IEFG method for potential and elastic problems

3.1. IEFG method for potential problems

In this section, we present the IEFG method for a 2D Poisson equation

$$\nabla^2 u + f(x) = 0, \qquad x \in \Omega, \tag{27}$$

$$u(x) = \overline{u}(x), \qquad x \in \Gamma_u, \tag{28}$$

$$\frac{\partial u(x)}{\partial n} = \overline{q}(x), \qquad x \in \Gamma_q, \tag{29}$$

where Ω is a 2D domain bounded by contour $\Gamma = \Gamma_u \cup \Gamma_q$, $u(x)$ is an unknown function, $f(x)$ is a known function $\overline{u}(x)$ is a Dirichlet boundary condition and $\overline{q}(x)$ is a Neumann boundary condition.

The Galerkin weak form of Eqs. (27)–(29) is

$$\int_\Omega (\nabla v^*)^T (\nabla u) d\Omega - \int_\Omega v^* . f d\Omega - \int_{\Gamma_q} v^* . \overline{q} d\Gamma_q = 0, \tag{30}$$

in which v^* is the test function.

From the approximation function (21), Eq. (30) can be written as follows:

$$[K] . \{u\} = \{F\}, \tag{31}$$

where

$$K_{IJ} = \int_\Omega \overline{\phi}_{I,x_1} \overline{\phi}_{J,x_1} + \overline{\phi}_{I,x_2} \overline{\phi}_{J,x_2} d\Omega, \tag{32}$$

$$F_I = \int_\Omega \overline{\phi}_I^T f d\Omega + \int_{\Gamma_q} \overline{\phi}_I^T \overline{q} d\Gamma_q. \tag{33}$$

In a steady-state heat transfer problem, which is a typical Poisson problem, u is the temperature field, $\overline{q}$ is the heat flux function and f is the internal heat generation.

3.2. Enforcement of essential boundary conditions

The lack of Kronecker delta property in the IEFG and EFG shape functions makes imposing the essential boundary condition difficult. For this reason, the essential boundary conditions cannot be imposed directly. Different methods are used to consider boundary conditions like Lagrange multipliers, coupling with the finite element and the penalty method. The advantages of the penalty approach are such that the size of the system of equations is constant and the modified stiffness matrix is still positively defined [18]. For these reasons, we use in this paper the penalty method to enforce the boundary conditions.

The new Galerkin weak form using the penalty method to introduce essential boundary conditions becomes

$$\int_{\Omega} (\nabla v^*)^T (\nabla u) d\Omega - \int_{\Omega} v^*.f d\Omega - \int_{\Gamma_q} v^*.\overline{q} d\Gamma_q + \frac{\alpha}{2} \int_{\Gamma_u} (v^* - \overline{v^*})^T (u - \overline{u}) d\Gamma_u = 0, \tag{34}$$

where α is the penalty factor chosen between 10^{4-13}*max (diagonal element of the stiffness matrix) [19].

Using Eq. (21), the final system matrix can be written as

$$([K] + [K^{\alpha}])\{u\} = \{F\} + \{F^{\alpha}\}, \tag{35}$$

where

$$K_{IJ} = \int_{\Omega} (\overline{\phi}_{I,x_1} \overline{\phi}_{J,x_1} + \overline{\phi}_{I,x_2} \overline{\phi}_{J,x_2}) d\Omega, \tag{36}$$

$$F_I = \int_{\Omega} \overline{\phi}_I f d\Omega + \int_{\Gamma_q} \overline{\phi}_i \overline{q} d\Gamma, \tag{37}$$

$$K^{\alpha}_{IJ} = \alpha \int_{\Gamma_u} \overline{\phi}_I \overline{\phi}_J d\Gamma_u, \tag{38}$$

$$F^{\alpha}_I = \alpha \int_{\Gamma_u} \overline{\phi}_I \overline{u} d\Gamma. \tag{39}$$

In the IEFG and EFG methods, the integration is made on elements: in our paper, the domain is dissociated into quadrilateral elements used only to evaluate integrals. In each element, four Gauss quadrature points are used.

3.3. IEFG method for elastic problem

Consider the following 2D problem in linear elasticity on the domain Ω that is bounded by the boundary Γ

$$\nabla \sigma + f = 0, \quad \text{in } \Omega, \tag{40}$$

in which σ is the stress tensor and f is the body force.

The corresponding boundary conditions are

$$u(x) = \overline{u}(x), \qquad x \in \Gamma_u, \tag{41}$$

$$\sigma.n = \overline{q}(x), \qquad x \in \Gamma_q, \tag{42}$$

where $\overline{u}(x)$ is the prescribed displacement vector on the boundary Γ_u, $\overline{q}(x)$ is the prescribed traction vector on the boundary Γ_q, and n is the unit outward normal to the boundary Γ. The principle of virtual work is

$$W = W_{\text{int}} - W_{\text{ext}} = 0, \tag{43}$$

where

$$W_{\text{int}} = \int_{\Omega} \langle \varepsilon^* \rangle \{\sigma\} \, d\Omega, \tag{44}$$

$$W_{\text{ext}} = \int_{\Omega} \langle v^* \rangle \{f\} \, d\Omega + \int_{\Gamma_q} \langle v^* \rangle \{\overline{q}\} \, d\Gamma_q, \tag{45}$$

where $\langle v^* \rangle$ is a kinematically admissible field and $\langle \varepsilon^* \rangle$ is the associated strain, knowing that

$$\langle v^* \rangle = \{v^*\}^T \qquad \text{and} \qquad \langle \varepsilon^* \rangle = \{\varepsilon^*\}^T.$$

In elasticity problem, the stress-strain relationship is

$$\{\sigma\} = [H] \{\varepsilon\}. \tag{46}$$

[H] is defined in plane stress, for example,

$$[H] = \frac{E}{(1-\vartheta^2)} \begin{bmatrix} 1 & \vartheta & 0 \\ \vartheta & 1 & 0 \\ 0 & 0 & \dfrac{1-\vartheta}{2} \end{bmatrix}, \tag{47}$$

where E is the Young modulus and ϑ is the Poisson ratio. Using Eq. (46) in Eq. (44) the internal work is given by

$$W_{\text{int}} = \int_{\Omega} \langle \varepsilon^* \rangle [H] \{\varepsilon\} \, d\Omega. \tag{48}$$

The strain can be expressed by

$$\{\varepsilon\} = [D] \{U\}, \tag{49}$$

where

$$[D] = \begin{bmatrix} \dfrac{\partial}{\partial x} & 0 \\ 0 & \dfrac{\partial}{\partial y} \\ \dfrac{\partial}{\partial y} & \dfrac{\partial}{\partial x} \end{bmatrix}, \tag{50}$$

$$\langle U \rangle = \langle u_1 \; v_1 \; u_2 \; v_2 \; \ldots \; u_n \; v_n \rangle. \tag{51}$$

Using Eq. (21) the displacement field can be written as follows:

$$\{U\} = \left[\overline{\phi}\right] \{U_n\}. \tag{52}$$

And the strain can then be expressed by

$$\{\varepsilon\} = [D]\left[\overline{\phi}\right]\{U_n\}, \tag{53}$$

where

$$\left[\overline{\phi}\right] = \begin{bmatrix} \overline{\phi_1} & 0 & \overline{\phi_2} & 0 & \dots & \overline{\phi_n} & 0 \\ 0 & \overline{\phi_1} & 0 & \overline{\phi_2} & \dots & 0 & \overline{\phi_n} \end{bmatrix}. \tag{54}$$

Let us take

$$[B] = [D]\left[\overline{\phi}\right] = \begin{bmatrix} \dfrac{\partial}{\partial x} & 0 \\ 0 & \dfrac{\partial}{\partial y} \\ \dfrac{\partial}{\partial y} & \dfrac{\partial}{\partial x} \end{bmatrix} \begin{bmatrix} \overline{\phi_1} & 0 & \overline{\phi_2} & 0 & \dots & \overline{\phi_n} & 0 \\ 0 & \overline{\phi_1} & 0 & \overline{\phi_2} & \dots & 0 & \overline{\phi_n} \end{bmatrix}. \tag{55}$$

Using (48), (53) and (55) the internal work is given as follows:

$$W_{\text{int}} = \int_{\Omega} \langle V_n^* \rangle [B]^T [H] [B] \{U_n\} \, d\Omega. \tag{56}$$

Using (45) and (52) the external work becomes as follows:

$$W_{\text{ext}} = \int_{\Omega} \langle V_n^* \rangle \left[\overline{\phi}\right]^T \{f\} \, d\Omega + \int_{\Gamma_q} \langle V_n^* \rangle \left[\overline{\phi}\right]^T \{\overline{q}\} \, d\Gamma_q. \tag{57}$$

The use of (57), (56) and (43) let us have the following final system to solve:

$$[K]\{U_n\} = \{F\}, \tag{58}$$

where

$$[K] = \int_{\Omega} [B]^T [H] [B] \, d\Omega, \tag{59}$$

$$\{F\} = \int_{\Omega} \left[\overline{\phi}\right]^T \{f\} \, d\Omega + \int_{\Gamma_q} \left[\overline{\phi}\right]^T \{\overline{q}\} \, d\Gamma_q. \tag{60}$$

The enforcement of the boundary conditions is made using the penalty method as discussed previously for potential problems.

4. Numerical examples

4.1. Diffusion equations

Two different examples are selected to demonstrate the precision and the speed of the IEFG method compared with EFG method. The results of these examples are compared with the analytical solutions.

4.1.1. Laplace's equation on a plate

A temperature field on a plate domain Ω, is governed by Laplace's equation [20]

$$\nabla^2 T(x, y) = 0, \qquad \forall x, y \in \Omega. \tag{61}$$

Dimensions and geometry of the domain are shown in Fig. 1.

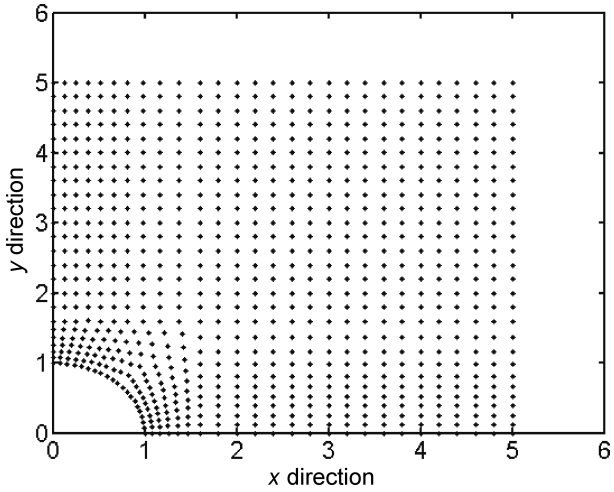

Fig. 1. Domain dimensions and geometry and node distribution.

The analytical temperature of this problem is given by

$$T(x,y) = e^x \sin y. \tag{62}$$

To impose the boundary conditions for this problem, the analytic solution given by Eq. (62) is used.

In the numerical procedure, an irregular distribution of nodes is used: the further we go away from the more density of nodes decreases. Node distribution is shown in Fig. 1. The penalty coefficient used to obtain the solution is 10^4 and the dimension of the domain of influence is $d = 1.2d_i$, so $a_c = 1.2$.

The results obtained using the IEFG and EFG methods are presented in many chosen directions. Indeed, temperature evolution is addressed for $x = 0$ mm, $x = 4$ mm and $y = 3$ mm respectively in Figs. 2, 4 and 6. The associated relative error evolutions, for $x = 0$ mm, $x = 4$ mm and $y = 3$ mm are respectively shown in Figs. 3, 5 and 7.

From these curves, it is clear that the IEFG method gives results in good agreement with the analytic ones relative error is always under 1.6%. In addition, from the relative error's curves, it seems that the EFG and IEFG methods have the same rate of precision. But when the computational speed is evaluated, it is found that the EFG method requires 13660 s (using a PC with

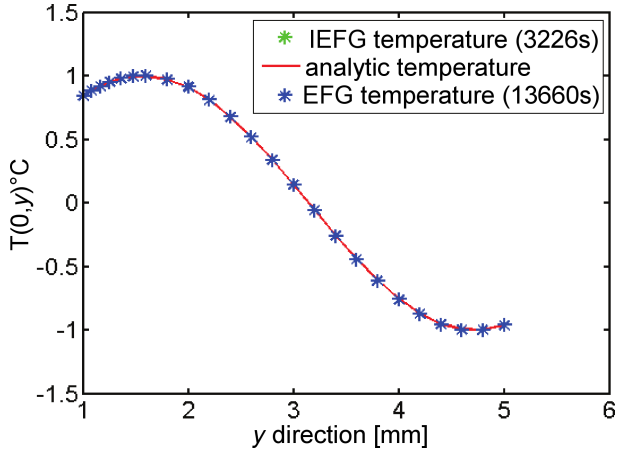

Fig. 2. Temperature evolution along y direction for $x = 0$ mm for EFG and IEFG superposed on analytic solution.

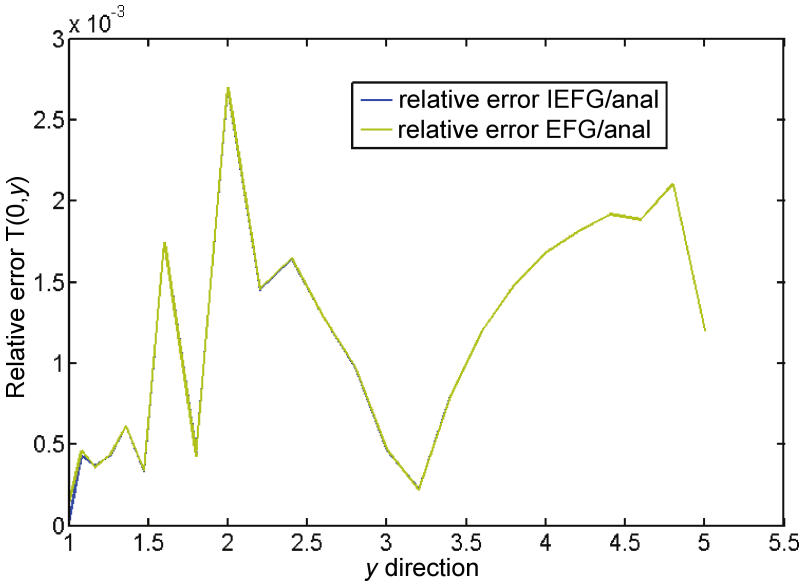

Fig. 3. Relative error evolution along y direction for $x = 0$ mm for the EFG and IEFG solutions.

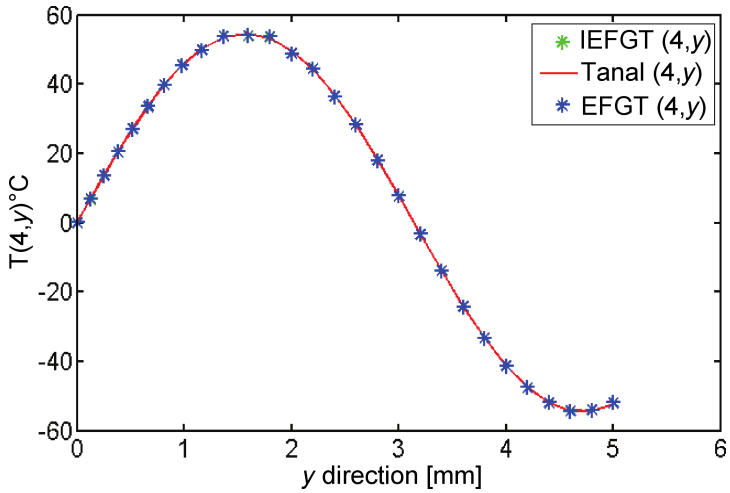

Fig. 4. Temperature evolution along y direction for $x = 4$ mm for EFG and IEFG superposed on analytic solution.

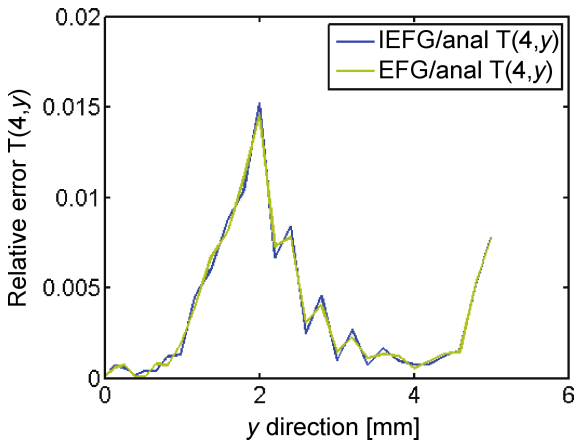

Fig. 5. Relative error evolution along y direction for $x = 4$ mm for the EFG and IEFG solutions.

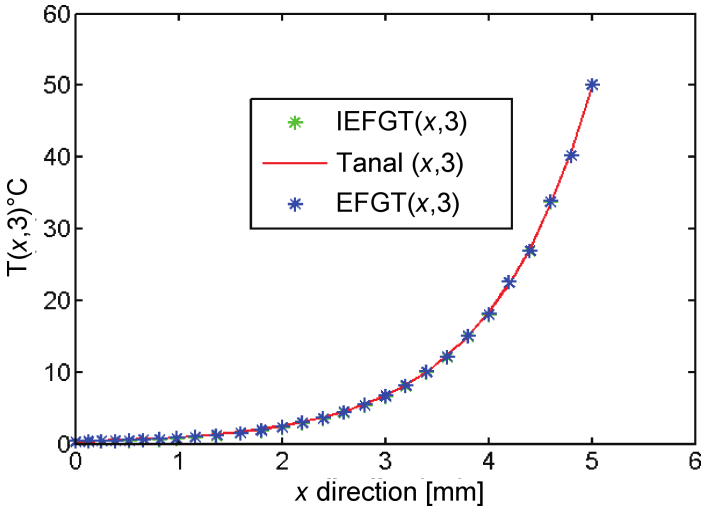

Fig. 6. Temperature evolution along x direction for $y = 3$ mm for the EFG and IEFG superposed on analytic solution.

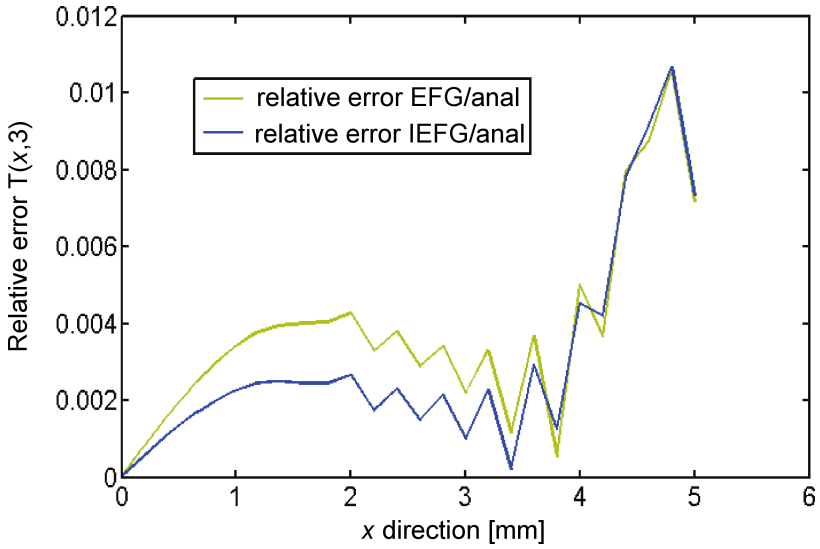

Fig. 7. Relative error evolution along x direction for $y = 3$ mm for the EFG and IEFG solutions.

RAM 16 Go Intel Core (TM) i7-3770 processor, and CPU@3.4Ghz), whereas the IEFG needs only 3226 s, and when the IEFG method is used, 76% of the CPU time is saved.

The relative error and the relative error norm, used in the paper, are calculated as follows:

$$\text{relative error} \quad R_i = \left| \frac{u_i^{\text{calc}} - u_i^{\text{analy}}}{\max(u^{\text{analy}})} \right|,$$

$$\text{relative error norm} = \left(\frac{\sum_i \left(u_i^{\text{calc}} - u_i^{\text{analy}} \right)^2}{\sum_i u_i^{\text{analy}^2}} \right)^{1/2}.$$

4.1.2. A diffusion equation with non-zero boundary conditions

A temperature field of a rectangular plate is given by this equation [21]:

$$\nabla^2 T = \frac{\partial^2 T}{\partial x_1^2} + \frac{\partial^2 T}{\partial x_2^2} = S(x_1, x_2)\, x_1 \in [0,1], \qquad x_2 \in [0,1]. \tag{63}$$

Knowing that

$$S(x_1, x_2) = 5.10^4 \left\{100\left[(1-x_1)^2 + x_2^2\right] - 2\right\} \exp\left\{-50\left[(1-x_1)^2 + x_2^2\right]\right\}, \tag{64}$$

the boundary conditions are

$$T(x_1, 0) = 100x_1 + 500\exp\left[-50\left(1 - x_1^2\right)\right] \qquad 0 < x_1 < 1, \tag{65}$$

$$T(x_1, 1) = 500\exp\left\{-50\left[\left(1 - x_1^2\right) + 1\right]\right\} \qquad 0 < x_1 < 1, \tag{66}$$

$$T(0, x_2) = 500\exp\left\{-50\left[\left(1 + x_2^2\right)\right]\right\} \qquad 0 < x_2 < 1, \tag{67}$$

$$T(1, x_2) = 100(1 - x_2) + 500\exp\left\{-50x_2^2\right\} \qquad 0 < x_2 < 1, \tag{68}$$

with the analytic solution

$$T(x_1, x_2) = 500\exp\left\{-50\left[\left(1-x_1^2\right) + x_2^2\right]\right\} + 100(1 - x_2)\, x_1. \tag{69}$$

For this equation, we present the evolution of the relative error norm obtained with the IEFG and EFG methods shown in Table 1, computed by varying the number of nodes in an increasing order of 11×11, 21×21 and 31×31.

Table 1. Relative error norm and CPU time of the EFG and IEFG methods at different number of nodes.

Nodes	EFG		IEFG	
	Relative error norm	CPU time	Relative error norm	CPU time
11*11	$3.41 \cdot 10^{-3}$	109 s	$3.4 \cdot 10^{-3}$	29.09 s
21*21	$3.712 \cdot 10^{-4}$	3735 s	$3.608 \cdot 10^{-4}$	1209 s
31*31	$1.707 \cdot 10^{-4}$	53678 s	$1.707 \cdot 10^{-4}$	35200 s

From Table 1, it appears that the IEFG and EFG methods have the same precision, about $1.7 \cdot 10^{-4}$ for a 31×31 node distribution. The use of the IEFG method reduces the CPU time of the full analysis by a 73% for a 11×11 node distribution, and 68% for a 21×21 node distribution; this improvement in a CPU time of analysis decreases to 35% for a 31×31 node distribution.

4.2. Elastic problems

To illustrate the efficiency of the IEFG method for 2D elasticity, two examples are studied. The problems are solved using regular node distribution.

4.2.1. Square plate under imposed displacement

This example considers a square plate of $[0,1] \times [0,1]$ under symmetric conditions at $x = 0$ and $y = 0$. A 0.1 mm displacement is imposed on the side of this plate where $y = 1$. The left side is traction-free (Fig. 8).

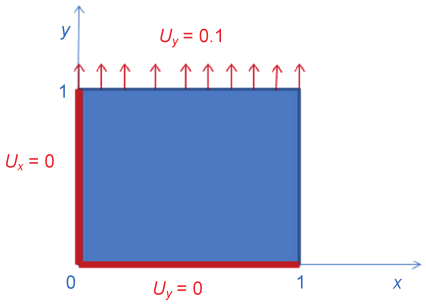

Fig. 8. A square plate under imposed displacement.

For this problem, a plane stress condition is assumed, and the material Young modulus $E = 200 \cdot 10^3$ MPa, and the Poisson ratio $\vartheta = 0.3$.

The analytic solution of this problem displacement is given as follows:

$$U_x = -0.03 * x, \tag{70}$$

$$U_y = 0.1 * y. \tag{71}$$

The normal stress of this problem is constant:

$$\sigma_{11} = 2 \cdot 10^4 \text{ MPa}. \tag{72}$$

To solve this problem, we used 11×11 nodes with a domain of influence size $d = 0.12$ mm. Both the EFG and IEFG methods give good results as shown in Figs. 9 and 10. For this case the use of

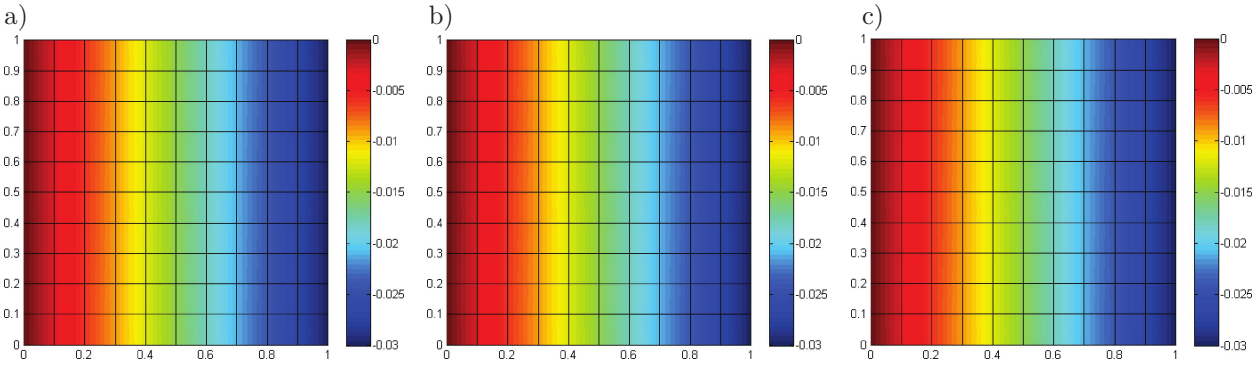

Fig. 9. U_x displacement obtained with IEFG (a), EFG (b) and analytically (c).

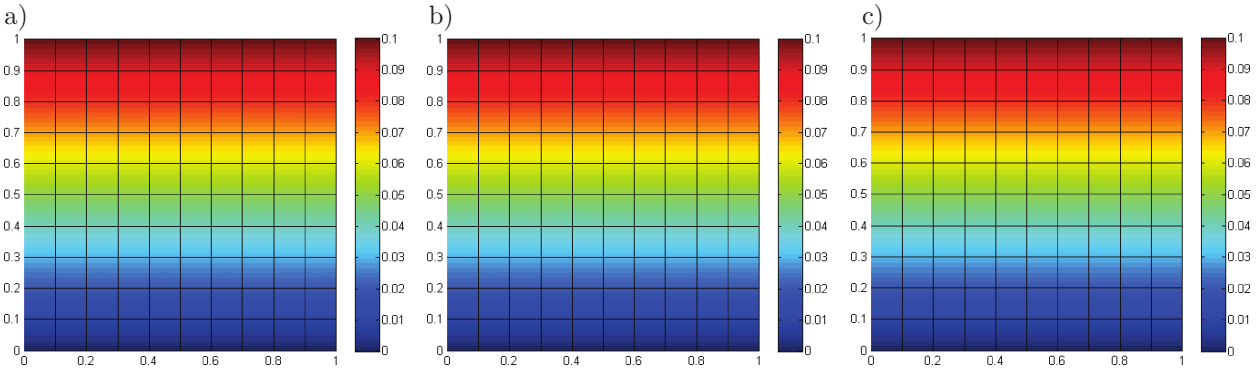

Fig. 10. U_y displacement obtained with IEFG (a), EFG (b) and analytically (c).

the IEFG method based on the IMLS approximation guaranties about 70% improvement in a CPU time of the complete analysis.

The relative errors between IEFG, EFG and analytic U_y $(x = 0.5, y)$ displacement are presented in Fig. 11. The IEFG and EFG methods have a close rate of error which is under $8 \cdot 10^{-5}\%$.

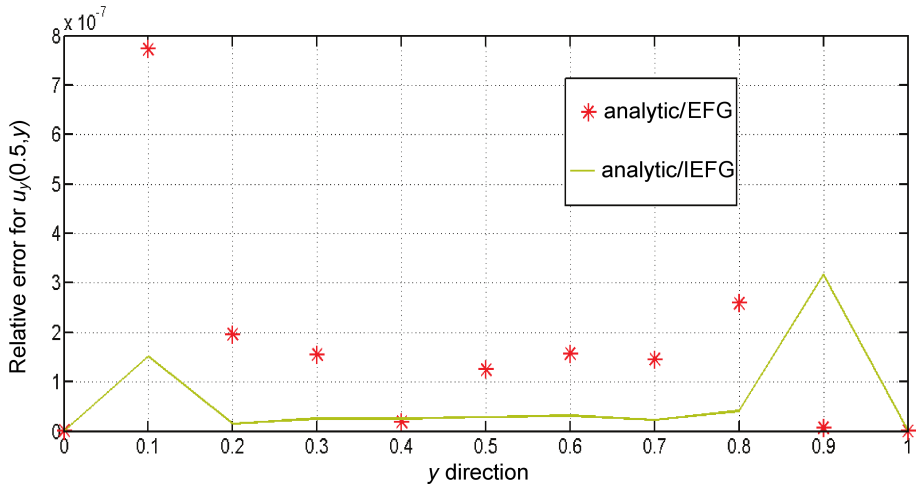

Fig. 11. Relative error for U_y $(x = 0.5, y)$.

4.2.2. Cantilevered beam

This example considers a beam subjected to a parabolic traction on the free end as shown in Fig. 12 [22].

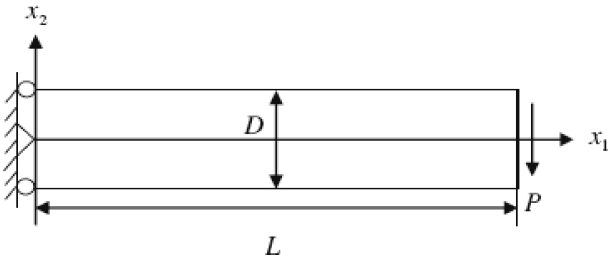

Fig. 12. Beam subjected to parabolic traction at the free end.

The length of the beam is $L = 50$ mm and the width of the beam is $D = 10$ mm. The imposed load is constant $P = 100$ N.

We treat the beam as a plane stress problem. The exact solution for this problem is

$$U_1 = -\frac{P * x_2}{6EI}\left[(6L - 3 * x_1) * x_1 + (2 + \vartheta) * \left(x_2^2 - \frac{D^2}{4}\right)\right], \tag{73}$$

$$U_2 = \frac{P}{6EI}\left[3\vartheta * x_2^2 (L - x_1) + (4 + 5\vartheta) * \left(D^2 * \frac{x_1}{4}\right) + (3L - x_1) * x_1^2\right], \tag{74}$$

$$\sigma_1 = \frac{-P (L - x_1) * x_2}{I}, \tag{75}$$

$$\sigma_2 = 0, \tag{76}$$

$$\sigma_{12} = \frac{P}{2I}\left(\frac{D^2}{4} - x_2^2\right), \tag{77}$$

where $I = \dfrac{D^3}{12}$ is the moment of inertia, $E = 30$ Mpa, and $\vartheta = 0.3$.

For this problem, the penalty factor used is $\alpha = 10^{10}$. The numerical and exact solutions of the displacements $U_1\left(x_1, \dfrac{D}{2}\right)$, $U_2\left(x_1, \dfrac{D}{2}\right)$ and stress $\sigma_1\left(\dfrac{L}{2}, x_2\right)$ are computed for different number of nodes: 17×13, 25×19 and 33×19. The CPU times of analysis and relative error norm for displacement and stress are presented in Table 2 for both the EFG and IEFG methods.

Table 2. Relative error norm for stress and displacement obtained with the EFG and IEFG methods.

Nodes	EFG			IEFG		
	Relative error norm		CPU time	Relative error norm		CPU time
	stress	displacement		stress	displacement	
17*13	$5.38 \cdot 10^{-3}$	$4.09 \cdot 10^{-5}$	510 s	$5.453 \cdot 10^{-3}$	$4.09 \cdot 10^{-5}$	99 s
25*19	3.6610^{-3}	$1.0745 \cdot 10^{-5}$	3912 s	$3.732 \cdot 10^{-3}$	$1.095 \cdot 10^{-5}$	523 s
33*19	1.910^{-3}	$7.401 \cdot 10^{-6}$	8739 s	$1.9 \cdot 10^{-3}$	$7.398 \cdot 10^{-6}$	960 s

As shown in Figs. 13, 14 and 15, it is clear that the IEFG method gives convergent results as well as number of nodes increases. The improvement of the CPU time obtained when the IEFG method is used is about 85% for a 25×19 node distribution and about 89% for a 33×19 node distribution. The relative error norm of displacement decreases from $4.09 \cdot 10^{-5}$ when a 17×13 node distribution is used to $7.39 \cdot 10^{-6}$ when a 33×19 node distribution is used.

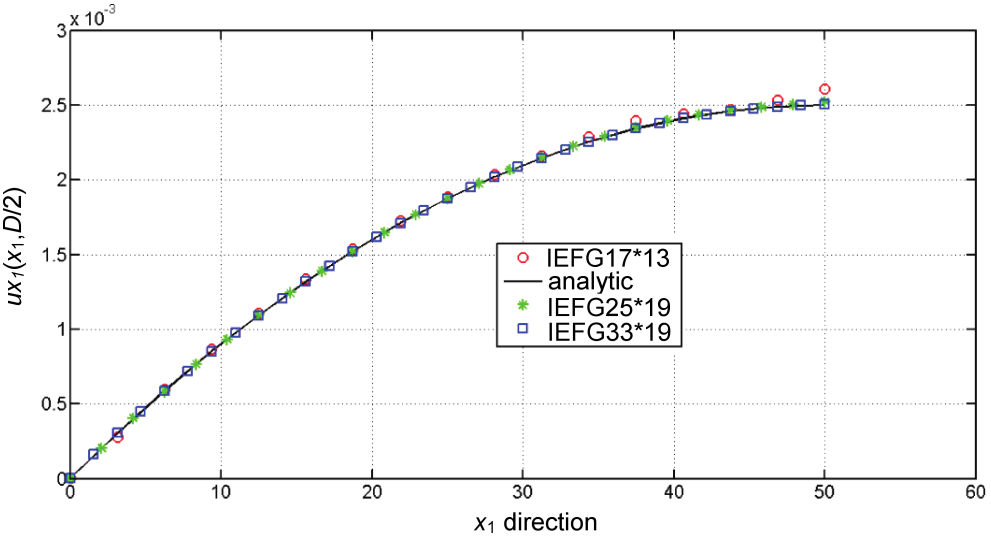

Fig. 13. ux_1 displacement (mm) at $x_2 = D/2$ for different number of nodes.

The relative error norm obtained for stress decreases from $5.45 \cdot 10^{-3}$, when a 17×13 node distribution is used, to $1.9 \cdot 10^{-3}$ for a 33×19 node distribution. For this elastic problem, the increase in the number of nodes does not decrease the improvement in the CPU time of the full analysis when the IEFG method is used. For the same rate of precision, as shown in Table 2, the use of the IEFG method allows a CPU time reduction of 85% in comparison with the EFG method.

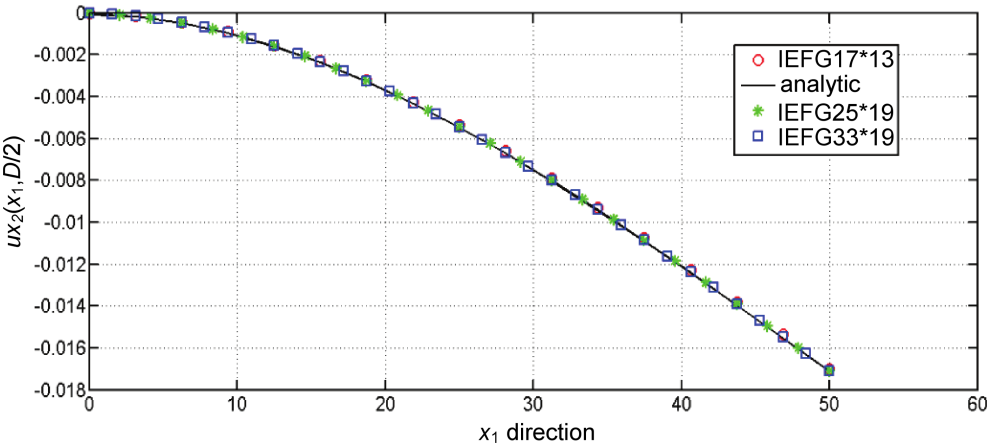

Fig. 14. ux_2 displacement (mm) at $x_2 = D/2$ for different number of nodes.

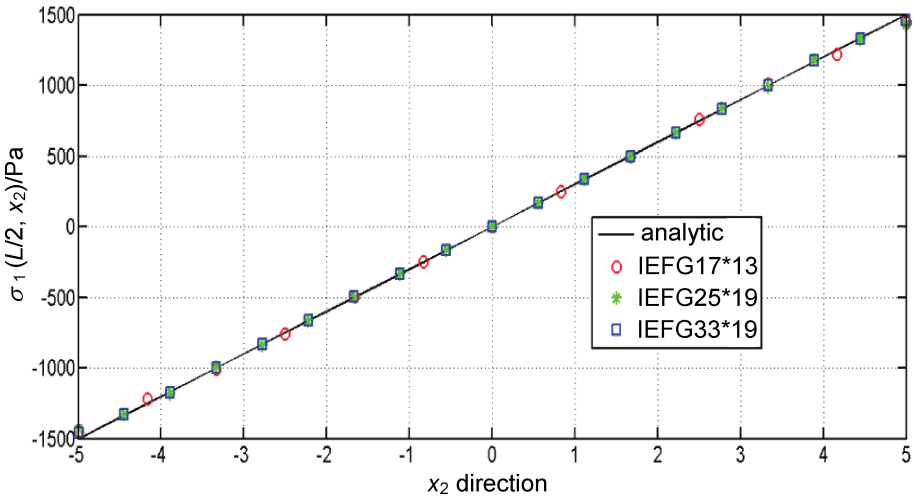

Fig. 15. Stress $\sigma_1\,(L/2, x_2)$ for different number of nodes.

4.2.3. Cylinder under internal pressure

In this section, a cylinder under internal pressure P is studied. Due to the symmetry of the proposed problem, we compute only a quarter of the cylinder as shown in Fig. 16.

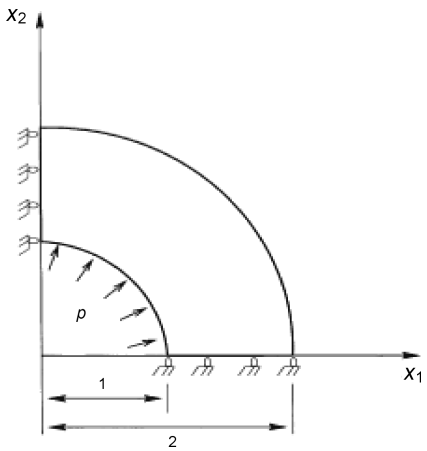

Fig. 16. A quarter of cylinder under internal pressure.

The thickness of the cylinder is equal to 1 mm, and the internal pressure $P = 1$ Pa. The properties of the material used are $E = 2 \cdot 10^5$ MPa and $\vartheta = 0.25$. Symmetry conditions are imposed for $x_1 = 0$ and for $x_2 = 0$.

The analytic solutions for this problem using polar coordinates (r, θ) are given as follows:

$$\sigma_{rr} = \frac{Pa^2}{(b^2 - a^2)}\left(1 - \frac{b^2}{r^2}\right), \tag{78}$$

$$\sigma_{\theta\theta} = \frac{Pa^2}{(b^2 - a^2)}\left(1 + \frac{b^2}{r^2}\right), \tag{79}$$

$$\sigma_{r\theta} = 0, \tag{80}$$

$$u_r = \frac{Pa^2}{E\,(b^2 - a^2)}\left[(1 - \vartheta)\, r + (1 + \vartheta)\,\frac{b^2}{r}\right], \tag{81}$$

$$u_\theta = 0. \tag{82}$$

For this problem, a distribution of 26×41 nodes is used, the size of the domain of influence d is not constant and it depends on a distance between two consecutive nodes d_i; so in this example $d = 1.8 d_i$. Penalty parameter that gives the most accurate results is $= 10^{11}$.

In the presented examples, the error realized with stresses is higher than the error realized with displacements. So, for this problem we focused on studying radial and tangential stresses to evaluate the precision and the speed of the IEFG method when compared to the EFG method. From Figs. 17 and 18 it is clear that the radial stresses for $\theta = 0$, $\theta = \pi/4$ and $\theta = \pi/2$ are in good agreement with

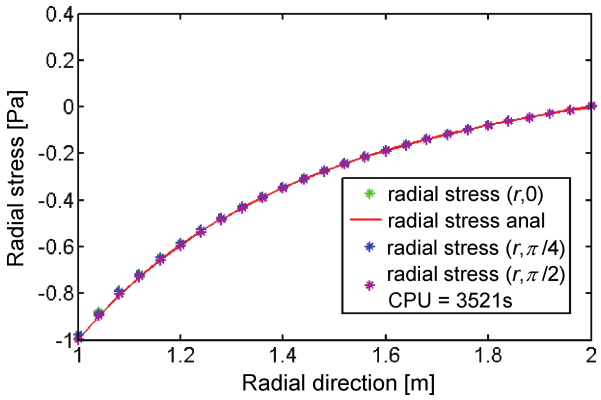

Fig. 17. Evolution of the radial stress for different directions: $\theta = 0$, $\theta = \pi/4$ and $\theta = \pi/2$ using the IEFG method.

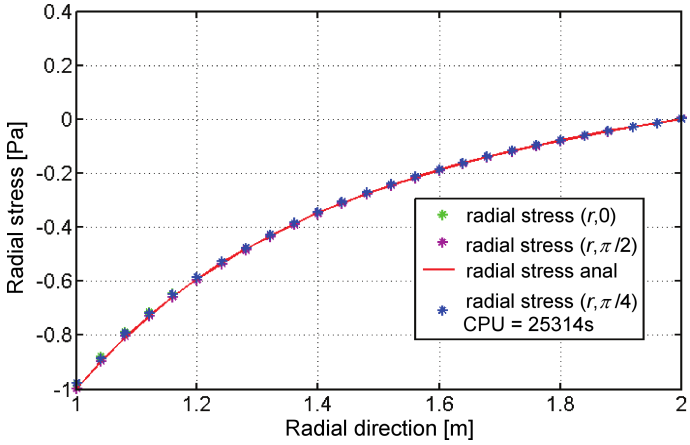

Fig. 18. Evolution of the radial stress for different directions: $\theta = 0$, $\theta = \pi/4$ and $\theta = \pi/2$ using the EFG method.

the analytic stress using both the IEFG method and EFG method. To quantify the relative error in all these chosen directions, Figs. 19 and 20 present respectively the relative error obtained when the IEFG method is used and the relative error obtained when the EFG method is used. From these figures, the relative error curves obtained with the IEFG method are similar to those obtained using the EFG method. The relative error is still under 2.5% for all values of chosen θ.

The same approach is applied to the tangential stress, which is shown in Figs. 21 and 22 respectively for the IEFG method and the EFG method. From these figures, the effectiveness of the IEFG

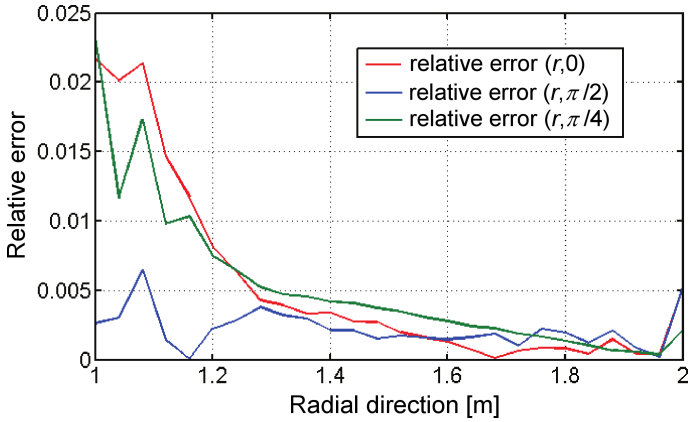

Fig. 19. Relative error for radial stress of different directions: $\theta = 0$, $\theta = \pi/4$ and $\theta = \pi/2$ obtained using the IEFG method.

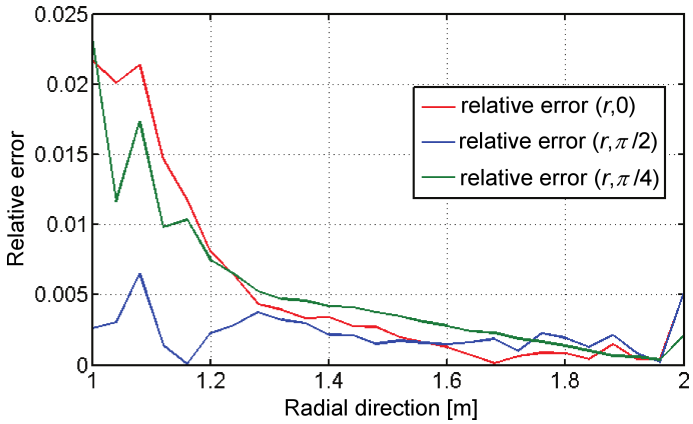

Fig. 20. Relative error for radial stress of different directions: $\theta = 0$, $\theta = \pi/4$ and $\theta = \pi/2$ obtained using the EFG method.

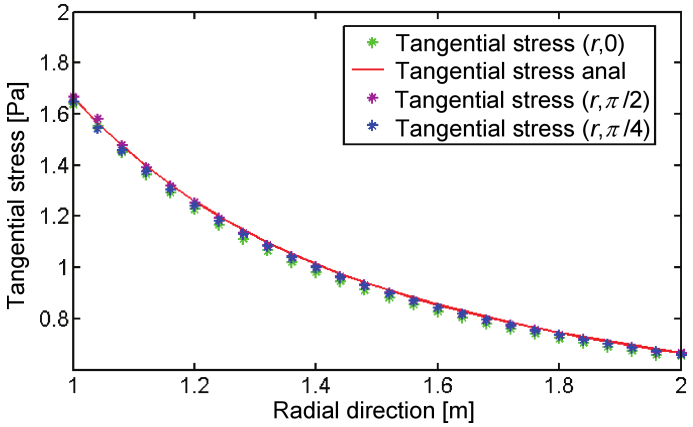

Fig. 21. Evolution of the tangential stress for different directions: $\theta = 0$, $\theta = \pi/4$ and $\theta = \pi/2$ using the IEFG method.

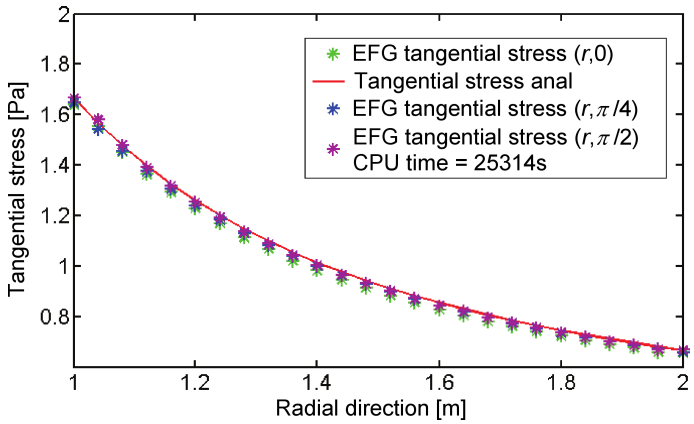

Fig. 22. Evolution of the tangential stress for different directions: $\theta = 0$, $\theta = \pi/4$ and $\theta = \pi/2$ using the EFG method.

method to provide a correct tangential stress is proved. In addition, the relative error, presented in Figs. 23 and 24, associated with these tangential stresses is still under 2.5% for both the IEFG and EFG methods.

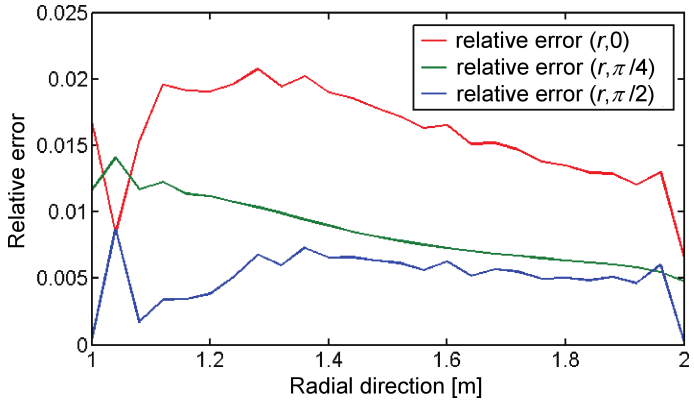

Fig. 23. Relative error of tangential stress for different directions: $\theta = 0$, $\theta = \pi/4$ and $\theta = \pi/2$ using the IEFG method.

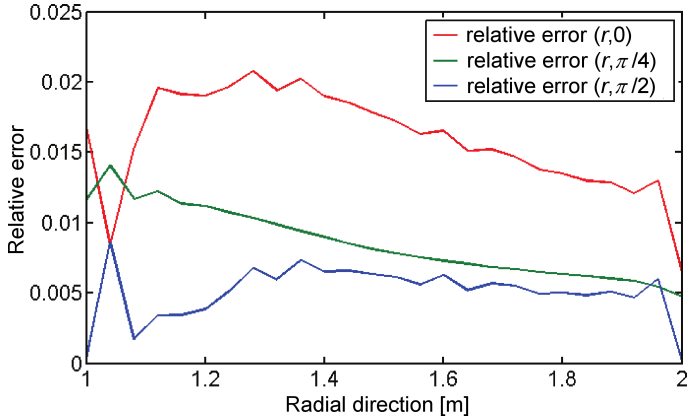

Fig. 24. Relative error of tangential stress for different directions: $\theta = 0$, $\theta = \pi/4$ and $\theta = \pi/2$ using the EFG method.

For all the above reasons, we can admit that the IEFG have the same precision as the EFG method. When a CPU time is considered, we find that for the same precision the IEFG method

needs 3521 s to give results, and the EFG method needs 25314 s to obtain a solution. Therefore, the use of the IEFG method allows to save about 86% from the CPU time when compared to the EFG method.

5. Conclusion

This paper proposes a comparison between the EFG method based on the MLS approximation and the IEFG method based on the IMLS approximation. A comparison is made for 2D potential problems and three elastic problems. The accuracy of the element-free methods is validated by comparing them with analytical solutions. The effect of the number of nodes on the convergence and result quality is examined. The convergence increases when the number of nodes increases. By using different examples it was demonstrated that the EFG method and the IEFG method have close or the same rate of precision. However, it is shown that, for the same precision, in case of the use of the IEFG method, at least 68% of the CPU time of the full analysis can be saved compared with the CPU time of the full analysis of the EFG method when a potential problem is treated. The improvement in a CPU time of the full analysis is about 86% with the IEFG method when an elastic problem is studied. From the studied problems, it is advised to use the IEFG method for solving 2D potential and elastic problems.

References

[1] Z. Zhang, K.M. Liew, Y. Cheng, Y.Y. Lee. Analyzing 2D fracture problems with the improved element-free Galerkin method. *Engineering Analysis with Boundary Elements*, **32**: 241–250, 2008.

[2] S.Y. Reutskiy. A meshless method for one-dimensional Stefan problems. *Applied Mathematics and Computation*, **217**: 9689–9701, 2011.

[3] N.F.M. Martins, M. Rebelo. A meshfree method for elasticity problems with interfaces. *Applied Mathematics and Computation*, **219**: 10732–10745, 2013.

[4] Y. Cheng, M. Chen. A boundary element-free method for linear elasticity. *Acta Mechanica Sinica*, **35**: 181–186, 2003.

[5] A. Karamanli, A. Mugan. Strong form meshless implementation of Taylor series method. *Applied Mathematics and Computation*, **219**: 9069–9080, 2013.

[6] R.A. Gingold, J.J. Monaghan. Smoothed particle hydrodynamics: theory and application to non-spherical stars. *Monthly Notices of the Royal Astronomical Society*, **181**: 375–389, 1977.

[7] L.B. Lucy. A numerical approach to the testing of the fission hypothesis. *Astronomical Journal*, **82**: 1013–1024, 1977.

[8] B. Nayroles, G. Touzot. Generalizing the finite element method: diffuse approximation and diffuse elements. *Computational Mechanics*, **10**: 307–318, 1992.

[9] T. Belytschko, YY. Lu, L. Gu. Element-free Galerkin methods. *International Journal for Numerical Methods in Engineering*, **37**: 229–256, 1994.

[10] C.A. Duarte, J.T. Oden. H-p clouds – an h-p meshless method. *Numerical Methods for Partial Differential Equations*, **12**: 673–706, 1996.

[11] S.N. Atluri, T.L. Zhu. A new meshless local Petrov-Galerkin (MLPG) approach in computational mechanics. *Computational Mechanics*, **22**: 117–127, 1998.

[12] Y.Y. Lu, T. Belytschko. A new implementation of the element free Galerkin method. *Computer Methods in Applied Mechanics and Engineering*, **113**: 397–414, 1994.

[13] He Zeng, Li Peng. Dispersion and pollution of the improved meshless weighted least-square (IMWLS) solution for the Helmholtz equation. *Engineering Analysis with Boundary Elements*, **35**: 791–801, 2011.

[14] R.J. Cheng, K.M. Liew. Analyzing modified equal width (MEW) wave equation using the improved element-free Galerkin method. *Engineering Analysis with Boundary Elements*, **36**: 1322–1330, 2012.

[15] Z. Zhang, Peng Zhao, K.M. Liew. Improved element-free Galerkin method for two-dimensional potential problems. *Engineering Analysis with Boundary Elements*, **33**: 547–554, 2009.

[16] I. Debbabi, Z. Sendi, H. BelHadj Salah. *Element Free and Improved Element Free Galerkin Methods for One and Two-Dimensional Potential Problems*. [In:] Design and Modeling of Mechanical Systems – II: 201–212, Springer International Publishing, 2015.

[17] P. Lancaster, K. Salkauskas. Surface generated by moving least squares methods. *Mathematics of Computation*, **37**: 141–158, 1981.

[18] T. Zhu, S.N. Atluri. A modified collocation method and a penalty formulation for enforcing the essential boundary conditions in the element free Galerkin method. *Comput. Mech.*, **21**: 211–222, 1998.
[19] G.R. Liu. *Mesh Free Methods: Moving Beyond the Finite Element Method*. CRC Press LLC, 2003.
[20] R. Hongping, Cheng Yumin. The interpolating element-free Galerkin (IEFG) method for two-dimensional potential problems. *Engineering Analysis with Boundary Elements*, **36**: 873–880, 2012.
[21] Prax Christian, Sadat Hamou. Mise en oeuvre d'une methode d'approximation diffuse adaptative pour la résolution des équations de diffusion et de transport. *Revue Générale de Thermique*, **37**: 39–48, 1998.
[22] Z. Zhang, K.M. Liew. Coupling of the improved element-free Galerkin and boundary element methods for two-dimensional elasticity problems. *Engineering Analysis with Boundary Elements*, **32**: 100–107, 2008.